

High-efficiency Corrosion Inhibition Performances of Substituted Phenanthroline Derivatives for Mild Steel in 1 M HCl

Yan-Li Lv¹, Fan-Yu Kong¹, Juan-Xia Chen¹, Li Zhou¹, Yan-Qiu Wang¹, Qi Wang^{1,2,*}, and Xiao Li^{1,*}

¹ School of Chemical Engineering, University of Science and Technology Liaoning, Anshan 114051, China

² School of Materials and Metallurgy, University of Science and Technology Liaoning, Anshan 114051, China

*E-mail: wangqiustl@yeah.net (Q. Wang); lixiao@ustl.edu.cn (X. Li)

Received: 16 July 2020 / Accepted: 18 September 2020 / Published: 31 October 2020

Two substituted 1,10-phenanthroline derivatives, i.e., 1,10-phenanthroline-4,7-diol (PHEN-OH) and 1,10-phenanthroline-5,6-diamine (PHEN-NH₂), were investigated in terms of their anticorrosive performance for mild steel in HCl media with the use of gravimetric, electrochemical and theoretical calculation methods. PHEN-OH exhibited more efficient corrosion inhibition than PHEN-NH₂. Essentially, both inhibitors, PHEN-OH and PHEN-NH₂, were confirmed to be predominately cathodic. Thermodynamic study indicated that PHEN-OH and PHEN-NH₂ spontaneously adsorbed on the surface of the test sample via two adsorption modes predominately by chemisorption, and the adsorption was consistent with the Langmuir adsorption isotherm. The inhibition mechanism was further verified via adsorption isotherms, UV-vis spectroscopy, and surface analysis (SEM-EDX). The relationship between the molecular structure of the inhibitors and the anticorrosive performance was determined by theoretical calculation, consistent with experimental data.

Keywords: Inhibitor; Adsorption; Acid media; Mild steel; Phenanthroline derivative

1. INTRODUCTION

Currently, the corrosion inhibition of mild steel has aroused great concern among scientific researchers. One of the best solutions is to adopt organic inhibitors, which exhibit universal features, including heteroatoms (N, O, S), multiple bonds, and aromatic systems and so on [1-3]. Based on those characteristics, various organic compounds have been developed, including surfactants [4,5], Schiff bases [6-8], aromatic heterocyclic compounds [9-11], natural extracts [12,13], and polymers [14,15],

which have been employed as efficient inhibitors to deal with the metallic corrosion that is common in an aggressive acidic environment.

1,10-Phenanthroline and its derivatives usually act as versatile polydentate ligands toward metal ions, which frequently have potential and diversified applications as chemosensors [16], biological probes [17], optoelectronic devices [18, 19] and pharmaceuticals [20]. As another promising application of corrosive inhibitors for metals in different media, few 1,10-phenanthroline derivatives have been consecutively developed. Misra and coworkers first investigated the inhibitive effect of 1,10-phenanthroline for mild steel in H_2SO_4 solution [21]. Subsequently, effective anticorrosive performances of 1,10-phenanthroline for cold rolled steel, mild steel and aluminum in different media were examined [22-24]. Through molecular design tactics, Obot and coworkers reported a series of imidazole-phenanthroline-based metal corrosion inhibitors in acidic solution [25-27]. Wang and coworkers reported a new imidazole[4,5-f][1,10] phenanthroline derivative and studied its corrosion inhibition for mild steel in the acidic media [28].

Evidently, 1,10-phenanthroline and its derivatives have manifested a bright tendency in anticorrosive performances for metal corrosion in acidic media due to the rigid planar structure, versatile ligand center and easy structure modification. In this article, we used two substituted 1,10-phenanthroline derivatives (Fig. 1), i.e., 1,10-phenanthroline-4,7-diol (PHEN-OH) and 1,10-phenanthroline-5,6-diamine (PHEN-NH₂), as the corrosion inhibitors for mild steel in 1 M HCl. Then, we investigated the anticorrosive effect by gravimetric and electrochemical methods and proposed thermodynamic models. The surface characteristics of the test samples were determined with scanning electron microscope (SEM). In addition, theoretical calculations based on density functional theory (DFT) and UV-vis spectroscopy were performed to clarify the adsorption mechanism. The substituents (-OH and -NH₂) are strong electron-donor groups with good water solubility, which contribute to the corrosion inhibition performance of PHEN-OH and PHEN-NH₂. As a result, both PHEN-OH and PHEN-NH₂ showed excellent corrosion inhibition performance for mild steel in acid media, and PHEN-OH exhibited more efficient corrosion inhibition than PHEN-NH₂.

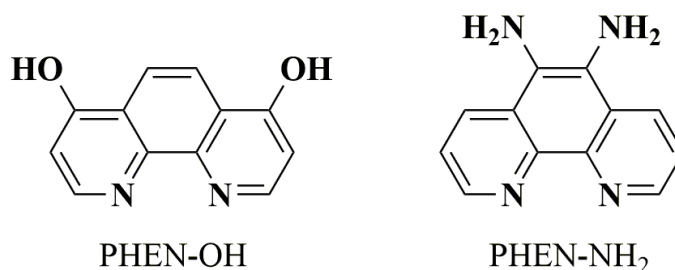


Figure 2. Chemical structures of the inhibitors PHEN-OH and PHEN-NH₂.

2. MATERIALS AND METHODS

2.1. Materials

The chemical composition (wt%) of the experimental specimens was as follows: Mn-0.50, Si-0.20, C-0.20, P-0.02, Cr-0.02, Cu-0.02, Ni-0.02 and Fe balance. The experimental test pieces were

manually ground by waterproof abrasive paper with different meshes (200, 400, 600, 800 and 1000) and successively rinsed with deionized H₂O and EtOH. Then, 1 M HCl solution (corrosive medium) was prepared based on the general procedure. PHEN-OH was of analytical grade, and PHEN-NH₂ was synthesized according to our previous procedures [29]. The chemical structures of PHEN-OH and PHEN-NH₂ are shown in Fig. 1.

2.2. Gravimetric method

The gravimetric method was performed with the weightlessness method in this study. The experimental sheets were immersed in the acidic solution with PHEN-OH and PHEN-NH₂ at different temperatures. Simultaneously, blank experiments were performed and compared with them. After a given time, the test pieces were removed from the corrosion system and processed with deionized H₂O, anhydrous ethanol, and cold air. Subsequently, the sheets were placed in the cabinet dryer and accurately weighed at room temperature.

The relative parameters, including the corrosion rate (C_w), efficiency of inhibitor (IE_w), and surface coverage (θ), were obtained using the following equations:

$$C_w = \frac{m - m_{inh}}{S \times t} \quad (1)$$

$$\theta = \frac{m - m_{inh}}{m} \quad (2)$$

$$IE_w(\%) = \frac{(m - m_{inh})}{m} \times 100 \quad (3)$$

where m and m_{inh} are the weightlessness value of the specimen for the blank hydrochloric acid solution and hydrochloric acid solution with corrosion inhibitor; S is the surface area of experimental sheets; and t is the immersion time.

2.3. Electrochemical tests

The electrochemical tests were performed with the Switzerland Autolab electrochemical workstation with three electrode configurations. The three-electrode system consisted of a platinum gauze electrode of 1.0 cm², a saturated calomel electrode and a working electrode (mild steel electrode with a working area of 1.0 cm²).

First, the electrodes were soaked in the corrosive medium for 45 minutes to achieve a steady open circuit potential (OCP), and E_{OCP} was obtained. Subsequently, the electrochemical impedance spectroscopy (EIS) of corrosion systems was measured in a certain frequency range from 100 kHz to 0.01 Hz. The corrosion inhibition efficiency (IE_r) was obtained via the formula [30]:

$$IE_r(\%) = \frac{R_{pi} - R_p}{R_{pi}} \times 100 \quad (4)$$

where R_{pi} and R_p are the impedances of the working electrode in the blank HCl solution and in the corrosion inhibitor, respectively.

The polarization curve experiment was performed under the following conditions: a potential of -1000 to 0 mv and a scanning rate of 0.2 mv s⁻¹.

The corrosion current density could be acquired through Tafel extrapolation. The corrosion inhibition efficiency ($IE_i\%$) was calculated as follows [30]:

$$IE_i(\%) = \frac{I - I_i}{I} \times 100 \quad (5)$$

$$\theta = \frac{I - I_i}{I} \quad (6)$$

where I and I_i are the corrosion current density of the working electrode in the blank HCl solution and the HCl solution with the corrosion inhibitor, respectively.

2.4. surface morphology analysis

After 8 h of immersion at ambient temperature in the blank HCl solution and HCl solution with corrosion inhibitor, corrosion morphologies of test specimens were observed using SEM integrated with energy-dispersive X-ray spectroscopy (EDX). The changes of chemical elements were analyzed through EDX.

2.5. UV-Vis spectroscopy technology

To investigate the adsorption characteristics of PHEN-OH and PHEN-NH₂ on the surface of test specimens, the UV-vis spectroscopy technology was applied. The mild steel samples were immersed into 1 M HCl solution with the inhibitor for 8 h. Then, the samples were removed and dried, and the forming film on the surface was carefully scraped off to record the UV-vis spectra by a Perkin-Elmer Lambda 900 spectrophotometer.

2.6. DFT calculations

To explore the effect of the molecular structure of inhibitors on the protection performance against mild steel corrosion, the structural parameters (E_{LUMO} and E_{HOMO}) of different inhibitors were calculated based on the density functional theory by the Gaussian 09 program package at the B3LYP/6-31G (d, p).

The theoretical indices of PHEN-OH and PHEN-NH₂ were calculated, which included lowest unoccupied molecular orbital (E_{LUMO}), highest occupied molecular orbital (E_{HOMO}), energy gap (ΔE), electronegativity (χ), dipole moment (μ), fraction of electrons transferred (ΔN), softness (σ) and hardness (η). The values of χ , ΔN , σ and η were obtained by the formula [30]:

$$\eta = -\frac{1}{2}(E_{HOMO} - E_{LUMO}) \quad (7)$$

$$\chi = -\frac{1}{2}(E_{HOMO} + E_{LUMO}) \quad (8)$$

$$\sigma = \frac{1}{\eta} \quad (9)$$

$$\Delta N = \frac{\chi_{Fe} - \chi_i}{2(\eta_{Fe} + \eta_i)} \quad (10)$$

where χ_{Fe} , χ_i and η_{Fe} , η_i are the negative electricity and hardness values of Fe and inhibitors PHEN-OH/PHEN-NH₂, respectively.

3. RESULTS AND DISCUSSION

3.1. Gravimetric method

The corrosion resistance of inhibitors is commonly evaluated by the weight-loss method, which is a classic method. The variations in IE_w with the concentration of inhibitors (PHEN-OH/PHEN-NH₂) for the test samples immersed in 1 M HCl at 30°C is plotted in Fig. 2.

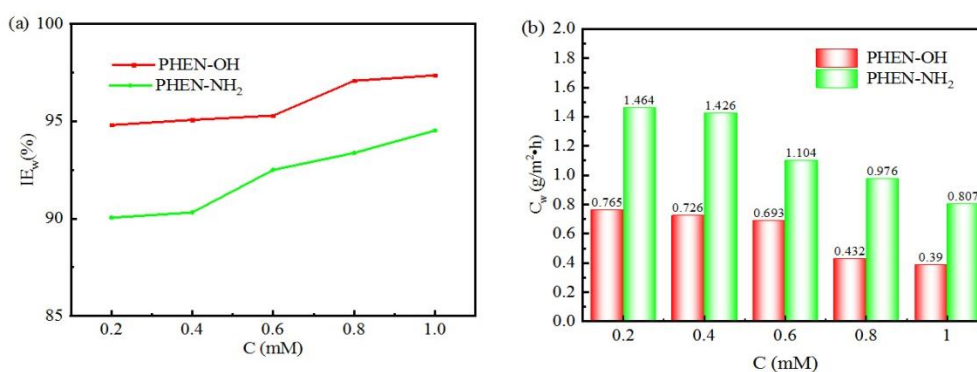
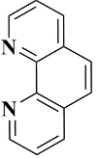
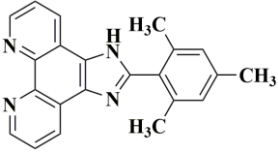
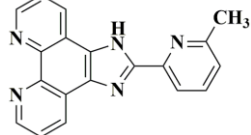
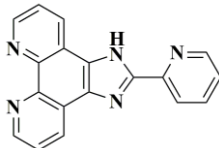
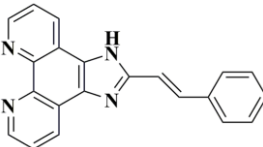


Figure 2. Variation of inhibition efficiency with concentration of inhibitors (PHEN-OH and PHEN-NH₂) for mild steel immersed in 1 M HCl at 30°C.

Fig. 2(a) shows that both PHEN-OH and PHEN-NH₂ can effectively block the corrosion of the steel test piece in hydrochloric acid solution. Furthermore, IE_w apparently rises with increasing concentrations, which may be ascribed to the increased surface coverage and adsorption of metal. The maximum IE_w values of PHEN-OH and PHEN-NH₂ are 97.6% and 94.5%, respectively, and the overall IE_w is in the order of PHEN-OH > PHEN-NH₂. The corrosion inhibition efficiency of PHEN-OH > PHEN-NH₂ is higher than the reported 1,10-phenanthroline derivatives in Table 1.

Table 1. 1,10-Phenanthroline derivative inhibitors and their maximum inhibition efficiency (IE_{wmax}) at different conditions for mild steel as determined by the gravimetric method.

Inhibitor	IE_{wmax} (%)	Condition	Reference
	97.6	1 M HCl, 30°C	this work
	94.5	1 M HCl, 30°C	this work

	92.1	1 M H ₂ SO ₄ , 30°C	21
	78.0	0.5 M H ₂ SO ₄ , 30°C	26
	72.0	0.5 M H ₂ SO ₄ , 30°C	27
	71.0	0.5 M H ₂ SO ₄ , 30°C	26
	84.2 (25°C) 97.6 (90°C)	0.5 M H ₂ SO ₄	28

The parameters (C_w and IE_w) in acidic solution with 1.0 mM PHEN-OH/PHEN-NH₂ at different temperatures are summarized in Table 2.

Table 2. Weight loss results of mild steel in 1 M HCl in the absence and presence of 1.0 mM PHEN-OH and PHEN-NH₂ at different temperatures.

Inhibitor	C_w (g/m ² ·h)					IE_w (%)				
	20°C	30°C	40°C	50°C	60°C	20°C	30°C	40°C	50°C	60°C
Blank	5.540	14.723	21.00	32.410	47.340	-	-	-	-	-
PHEN-OH	0.381	0.390	0.798	1.250	3.220	95.04	97.35	96.20	96.14	93.20
PHEN-NH ₂	0.283	0.807	1.048	1.327	2.967	94.89	94.52	95.01	95.91	93.73

As shown in Table 2, the corrosion rate, C_w , increases with increasing temperature, which indicates that the dissolution rate of metal improves with the increase in temperature. The significantly reduced C_w values of PHEN-OH and PHEN-NH₂ *versus* those of the blank indicate that PHEN-OH and PHEN-NH₂ are effective corrosion inhibitors in the current working system. The descending corrosion inhibition phenomenon following the increase in temperature is associated with the thermal desorption of PHEN-OH/PHEN-NH₂ on the metal surface [31, 32]. All IE_w values are more than 93% in a wide range of temperature (20-60 °C), which demonstrates that in the acidic environment, both PHEN-OH and PHEN-NH₂ are effective corrosion inhibitors for mild steel.

3.2. Adsorption isotherm and thermodynamics

The study of thermodynamics is of great significance in revealing the adsorption mechanism of inhibitors on the surface of the test piece. The adsorption process of PHEN-OH/PHEN-NH₂ inhibitors at 30°C was described by the Langmuir adsorption isotherm, which fitted well with the experimental results of weightlessness.

The Langmuir adsorption isotherm can be expressed as follows [33]:

$$\frac{C}{\theta} = \frac{1}{K_{ads}} + C \quad (11)$$

where K_{ads} and C are the adsorption equilibrium constant and inhibitor concentration, respectively.

In Fig. 3, both Langmuir adsorption plots are in a straight line, and the linear correlation coefficients are 0.9996 and 0.9995 for PHEN-OH and PHEN-NH₂, respectively, which indicates that both PHEN-OH and PHEN-NH₂ are well adsorbed according to the Langmuir isotherm. It is well known that the inhibitors with larger K_{ads} have more powerful adsorption action [33]. The K_{ads} of inhibitors PHEN-OH and PHEN-NH₂ (Table 3) shows that the current inhibitive molecules can strongly adsorb on the test piece, and PHEN-OH absorbs better.

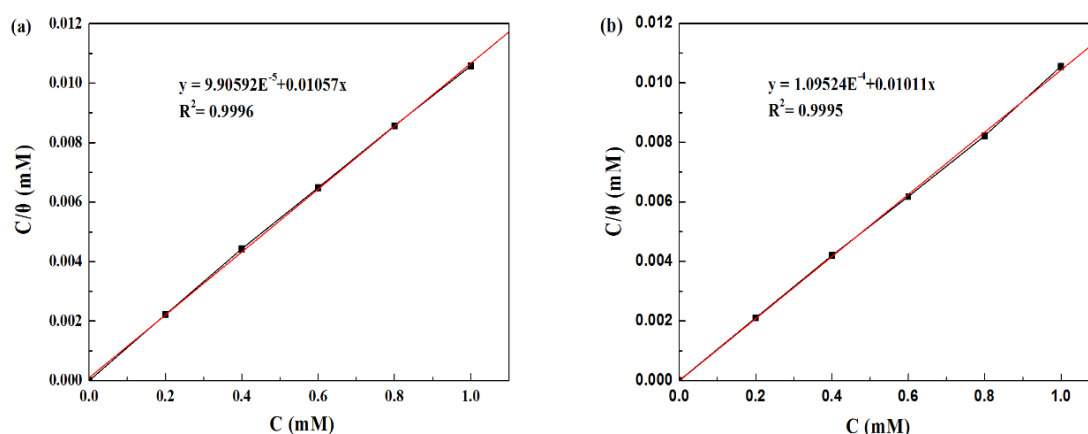


Figure 3. Langmuir adsorption plots for mild steel in 1 M HCl with different concentration of PHEN-OH and PHEN-NH₂ at 30°C.

Table 3. Thermodynamics parameters obtained from the Langmuir adsorption isotherm for PHEN-OH and PHEN-NH₂ at 30°C.

Inhibitor	K_{ads} (M ⁻¹)	ΔG_{ads} (KJ/mol)	E_a (KJ/mol)	ΔH (KJ/mol)	ΔS (KJ/mol)
Blank	-	-	33.9	-32.03	-110.87
PHEN-OH	10094.97	-32	59.9	-59.24	-115.65
PHEN-NH ₂	9130.49	-32	56.5	-47.58	-118.72

The thermodynamic parameters, including ΔH (standard enthalpy of activation), ΔG_{ads} (standard free energy of adsorption), ΔS (entropy of activation), and E_a (activation energy), are calculated as follows [34]:

$$\Delta G_{\text{ads}} = -RT \ln(55.5K_{\text{ads}}) \quad (12)$$

$$\ln C_w = -\frac{E_a}{RT} + \ln A_r \quad (13)$$

$$\ln\left(\frac{C_w}{T}\right) = -\frac{\Delta H}{RT} + \ln\left(\frac{R}{Nh}\right) + \frac{\Delta S}{R} \quad (14)$$

where R , T , A_r , h , and N are the universal gas constant, thermodynamic temperature, Arrhenius pre-exponential factor, Planck's constant, and Avogadro's number, respectively, and 55.55 is the molar concentration of water.

The $\Delta G_{\text{ads}}/\Delta H$ value is negative, which demonstrates a spontaneous exothermic behavior during the adsorption process. ΔG_{ads} is used to illustrate the absorbing type of inhibitors. When the absolute value of ΔG_{ads} is less than 20, physical adsorption occurs between the metal surface and the inhibitor; when the absolute value of ΔG_{ads} is more than 40, chemical absorption occurs. Both physical and chemical adsorption exist when the absolute value is 20-40 [35, 36]. ΔG_{ads} of PHEN-OH and PHEN-NH₂ is calculated as -32 KJ/mol, which indicates that the inhibitors PHEN-OH and PHEN-NH₂ can suppress the metal corrosion through two adsorption modes with mainly chemical adsorption. Table 3 demonstrates an increase in E_a in the presence of PHEN-OH and PHEN-NH₂, and E_a follows the order of E_a (PHEN-OH) > E_a (PHEN-NH₂), which suggests that the corrosion behavior is difficult to occur in the presence of PHEN-OH/PHEN-NH₂, and the corrosion rate increases with E_a . Moreover, the negative ΔH reveals the exothermal property of adsorption for mild steel, while the negative ΔS value suggests that associative instead of dissociative action occurs in the rate-determining step [37].

3.3. Electrochemical measurement

The electrochemical test must be performed under steady-state conditions. Before each electrochemical test, OCP must achieve stable values after approximately 45 minutes both without and with PHEN-OH/PHEN-NH₂ inhibitors (Fig. 4).

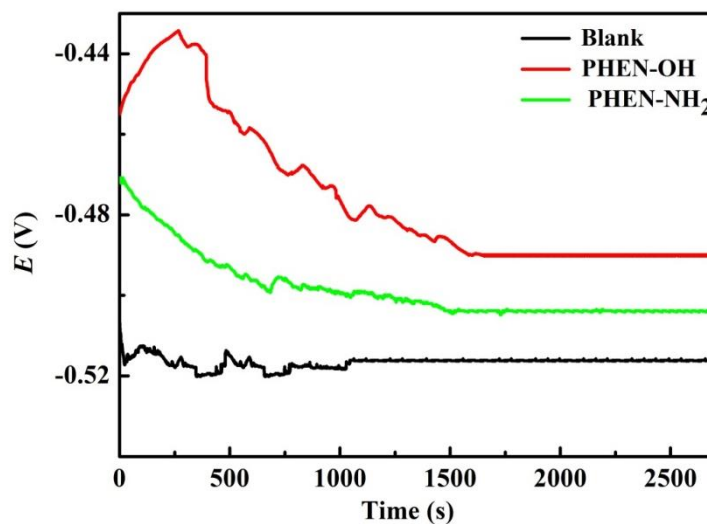


Figure 4. OCP curves of Blank and 1.0 mM inhibitors for MS in HCl at room temperature.

3.4. Potentiodynamic polarization study

The polarization curves of mild steel in 1 M HCl solution with or without PHEN-OH/PHEN-NH₂ at room temperature are shown in Fig. 5.

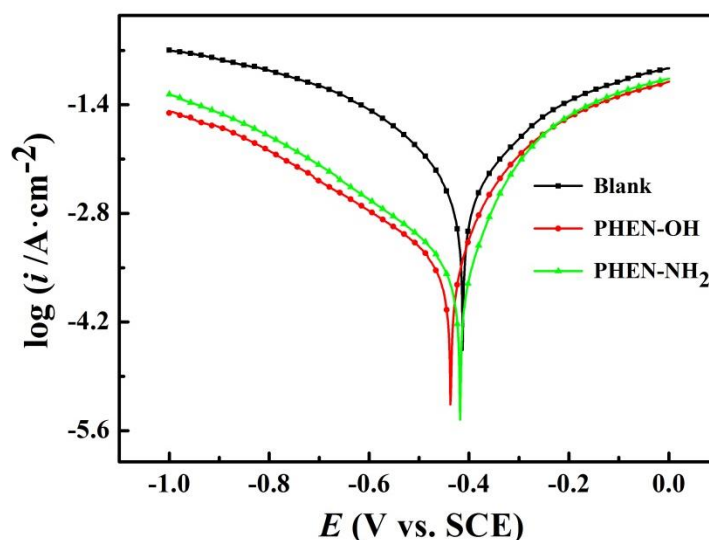


Figure 5. Potentiodynamic polarization plots for mild steel in 1 M HCl in the absence and presence of PHEN-OH (a) and PHEN-NH₂ (b) at room temperature.

To further investigate the corrosion kinetics of mild steel in HCl media, the electrochemical parameters, which are listed in Table 4, including I_{corr} (corrosion current density), E_{corr} (corrosion potential), β_c and β_a (cathodic and anodic Tafel constants), IE_i (inhibition efficiency) and θ (surface coverage), were surveyed.

Table 4. Potentiodynamic polarization parameters of mild steel in 1 M HCl in the absence and presence of PHEN-OH and PHEN-NH₂ at different concentrations.

Inhibitor	C (mM)	E_{corr} (mV vs. SCE)	β_c (mV dec ⁻¹)	β_a (mV dec ⁻¹)	I_{corr} ($\mu\text{A cm}^{-2}$)	IE_i (%)
Blank	-	-412	41	38	398.1	-
	0.2	-452	25	26	63.1	84.2
	0.4	-442	23	21	39.8	90.0
PHEN-OH	0.6	-440	60	21	25.1	93.7
	0.8	-436	39	26	15.8	96.0
	1.0	-437	33	27	10.0	97.5
	0.2	-402	26	25	100.0	74.9
PHEN-NH ₂	0.4	-395	29	22	50.1	87.4
	0.6	-413	42	20	31.6	92.1
	0.8	-407	30	26	25.6	93.6
	1.0	-409	32	31	15.8	96.0

The results in Fig. 5 and Table 4 indicate that both cathodic and anodic reactions of corrosion are reduced, and the cathodic effect was dominant in HCl media with different concentrations of PHEN-OH/PHEN-NH₂.

Moreover, the corrosion current density distinctly decreases with the addition of PHEN-OH and PHEN-NH₂, which suggests that both metal dissolution reaction and hydrogen evolution reaction are effectively inhibited. The cathodic polarization curves are shown in Fig. 5, which show that the hydrogen evolution mechanism is hardly changed after the addition of PHEN-OH/PHEN-NH₂. Table 4 shows that all displacements of E_{corr} in the range of 17–40 mV are less than 85 mV *versus* SCE, which indicates that both PHEN-OH and PHEN-NH₂ act as mixed-type inhibitors [38, 39]. Furthermore, the slight alteration in β_c and β_a compared with those of the blank is witnessed, and the variation of β_c is more obvious, which further demonstrates that PHEN-OH and PHEN-NH₂ can inhibit the metal corrosion with predominately a cathode-based inhibitive effect. Corrosion inhibition increases with the increase in PHEN-OH/PHEN-NH₂, and the highest IE_i values of 97.5% and 96.0% at optimized concentration (1.0 mM) are obtained.

3.5. Electrochemical impedance spectroscopy

The EIS technique is a valid method to obtain information about the inhibition process. The Bode plots, Nyquist plots and equivalent circuit for mild steel in 1 M HCl with and without inhibitors PHEN-OH and PHEN-NH₂ under steady-state conditions are shown in Fig. 6.

The results in Fig. 6 (a) and Fig. 6 (c) indicate that after the addition of the inhibitor PHEN-OH/PHEN-NH₂, the impedance response of mild steel was significantly changed, and the semicircle was enlarged in the order of PHEN-OH > PHEN-NH₂. There is only one capacitive reactance arc on EIS at E_{corr} , which is a result of the charge transfer and indicates one time constant. In addition, all impedance arcs are not strictly ordered semicircles, probably the inhomogeneity and roughness of the test piece surface and the adsorption of the inhibitor [40, 41].

The relevant parameters derived from Nyquist plots, including R_s , R_p , R_{ct} , Y and the inhibitive efficiency (IE_r), are calculated and shown in Table 5.

The equivalent-circuit model for the corrosion system provides some insight into the EIS data. All corrosion problems in the system are simulated using an appropriate equivalent circuit, which verifies that the charge-transfer process greatly hinders the interfacial reaction of acid/metal. R_s and R_{ct} in the equivalent circuit indicate the solution impedance and transfer impedance, respectively. The CPE is a constant-phase component instead of an electric double-layer capacitor and must be fitted according to the experimental results [42]. The CPE was calculated using formula (15):

$$Z_{\text{CPE}} = \frac{1}{Y_0(j\omega)^n} \quad (15)$$

where Y_0 , j , n and ω are the CPE constant, imaginary number, phase shift ($-1 \leq n \leq 1$) and angular frequency, respectively. CPE is closely related to n , and CPE can be considered to be the capacitance, resistance, and inductance when n is equal to 1, 0, and -1, respectively. n is the main index to indicate the dissolution mechanism. As shown in Table 5, n is 0.7–1.0, which has no obvious change after PHEN-OH/PHEN-NH₂ at different concentrations was added, which

demonstrates that the dissolution mechanism is controlled by the charge-transfer process in the absence and presence of PHEN-OH/PHEN-NH₂ at different concentrations [10].

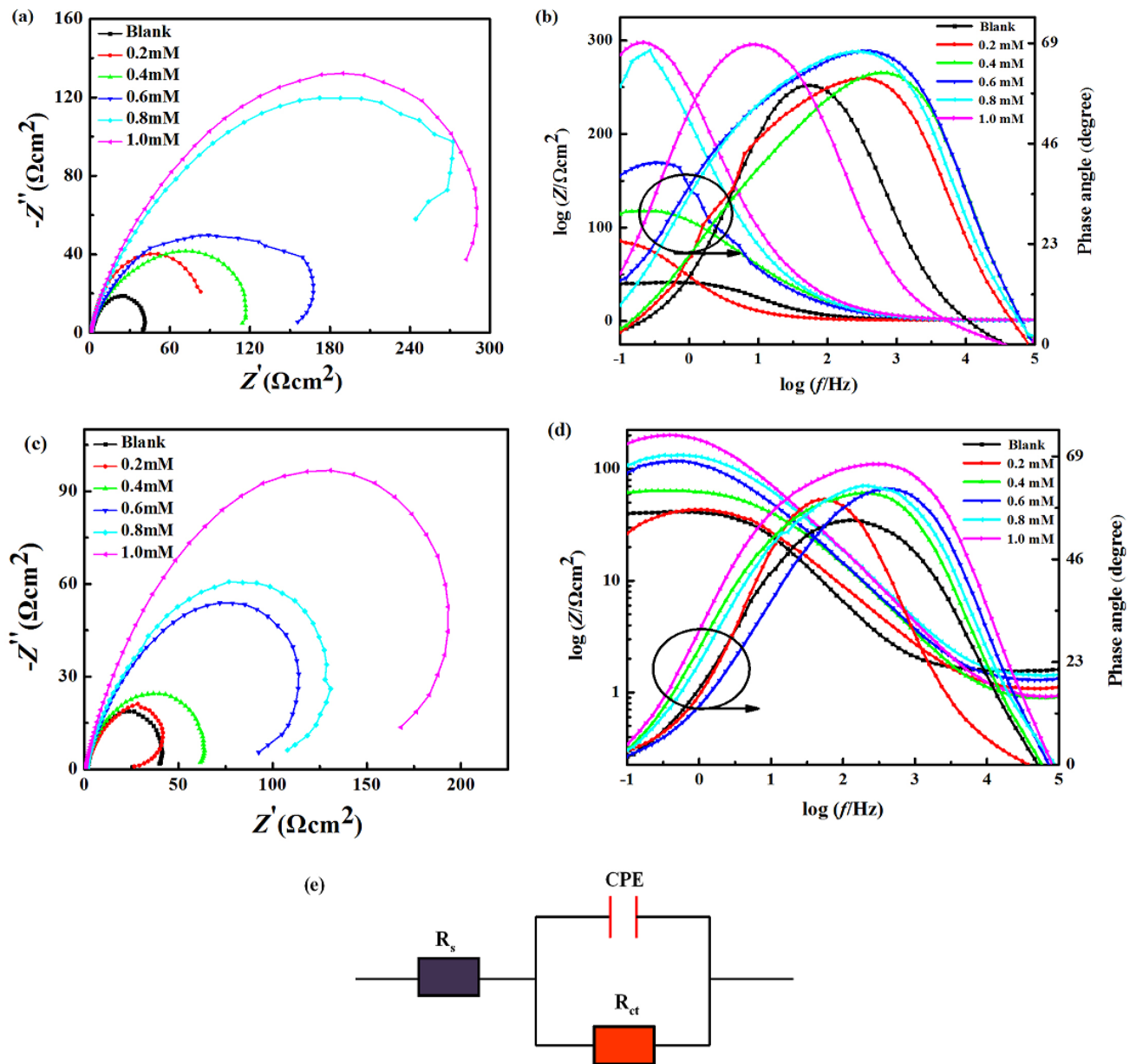


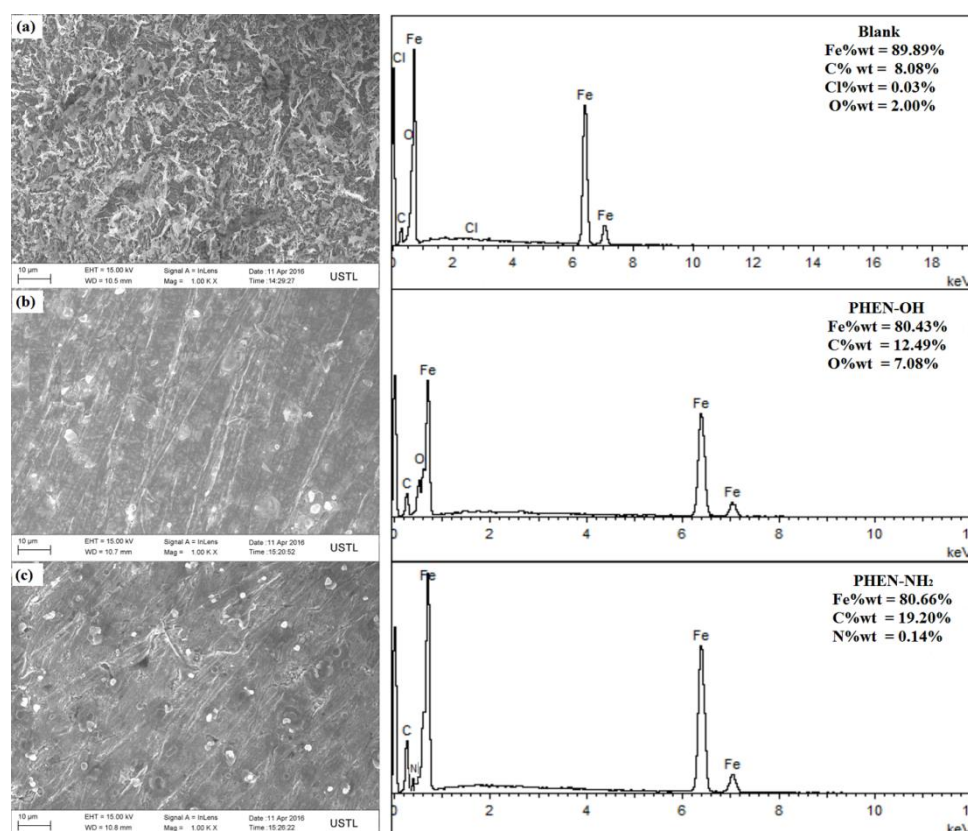
Figure 6. Nyquist, Bode/phase impedance plots and equivalent circuit for mild steel in 1 M HCl in the absence and presence of PHEN-OH and PHEN-NH₂ at room temperature. ((a) Nyquist plots of PHEN-OH; (b) Bode/Phase plots of PHEN-OH; (c) Nyquist plots of PHEN-NH₂; (d) Bode/Phase plots of PHEN-NH₂; (e) equivalent circuit)

In Table 5, R_p gradually increases with increasing concentrations, which reveals that both PHEN-OH and PHEN-NH₂ can restrict the charge transfer by adsorbing on the electrode surface. The trend of Y is opposite, mainly due to the replacement of H₂O by PHEN-OH/PHEN-NH₂ on the test piece surface [43]. In addition, the anticorrosive performance becomes more remarkable with increasing concentration and follows the order of PHEN-OH > PHEN-NH₂.

Table 5. The electrochemical impedance parameters of mild steel in the absence and presence of PHEN-OH and PHEN-NH₂ in 1 M HCl.

Inhibitor	C (mM)	R_p ($\Omega \cdot \text{cm}^2$)	R_s ($\Omega \cdot \text{cm}^2$)	R_{ct}		Y ($\times 10^4 / \Omega \cdot \text{cm}^2$)	n	$IE_r(\%)$
				($\Omega \cdot \text{cm}^2$)	Error(%) $\times 10^{-3}$			
Blank	0	38.7	12.0	26.7	2.271	16.04	0.9998	-
	0.2	89.6	13.6	76.0	7.235	5.14	0.77935	56.8
	0.4	121.3	21.9	99.4	6.536	2.94	0.9957	68.1
PHEN-OH	0.6	163.4	2.8	160.6	1.074	2.18	0.7712	76.3
	0.8	274.5	9.1	265.4	2.327	1.95	0.8253	85.9
	1.0	297.8	20.4	277.4	7.341	1.02	0.8035	87.0
	0.2	47.9	1.1	46.8	1.886	4.95	0.7508	19.2
PHEN-NH ₂	0.4	63.4	0.9	62.5	1.523	3.03	0.7444	39.0
	0.6	117.9	8.4	109.5	3.248	2.79	0.8707	67.2
	0.8	134.1	11.0	123.1	6.571	1.97	0.9746	71.1
	1.0	194.3	6.3	188.0	1.843	1.16	0.8527	80.1

3.6. Surface analysis

**Figure 7.** SEM micrographs and EDX spectra of mild steel surface after 8 h immersion time in 1 M HCl: (a) without the inhibitor; (b) with 1.0 mM PHEN-OH; (b) with 1.0 mM PHEN-NH₂.

The corrosion morphology of the test piece is observed by the German Zeiss-IGMA HD SEM with EDX after the test piece had been immersed in HCl media with and without PHEN-OH/PHEN-

NH₂ at 30°C for 8 h. The test piece surface without PHEN-OH/PHEN-NH₂ is severely corroded with cracks and pits because of the aggressive acidic media, as shown in Fig. 7(a). In comparison, after the addition of PHEN-OH/PHEN-NH₂, few cracks and pits are observed, probably because a protective film is formed on the surface of the test piece to isolate the aggressive acidic environment. Furthermore, the regular and polishing lines in Fig. 7(b) indicate the better anticorrosive performance of PHEN-OH.

The EDX studies suggest that Fe still has an irreplaceable status among the element composition of the test piece surface. After 8 h of immersion, the element composition proportion on the surface of the test piece is different. Compared with the blank HCl solution, for the test piece surface immersed in inhibitive solution, the C and O contents increase, and N element is present (Fig. 7), which demonstrates that both PHEN-OH and PHEN-NH₂ can adsorb on the test piece surface to prevent acid damage.

3.7. UV-vis spectroscopy study

To confirm whether the complex (inhibitor + Fe) has been formed, Fig. 8 shows UV-vis adsorption spectra from the corrosive solution in the presence of 1.0 mM PHEN-OH/PHEN-NH₂ before the test piece immersion and the scraped-off product on the surface of the immersed test piece.

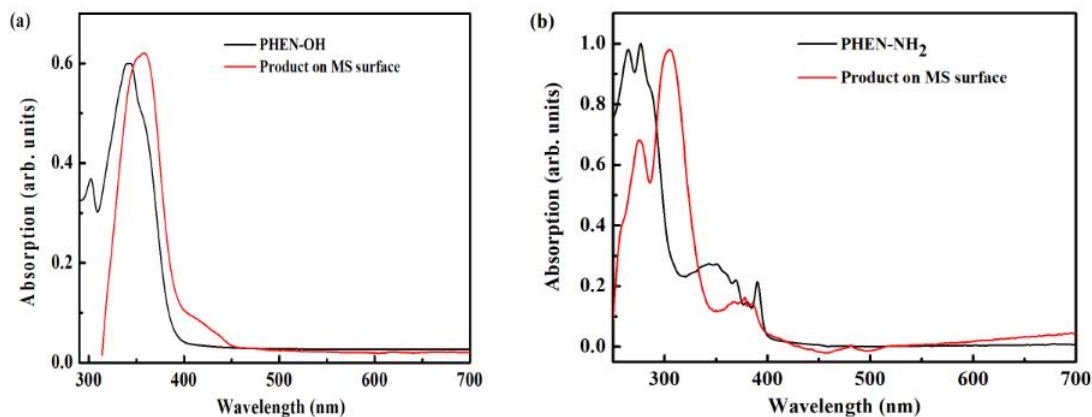


Figure 8. UV-vis absorption spectra of the solutions containing 1 M HCl + PHEN-OH (a) / PHEN-NH₂ (b) before and after immersion of test piece for 8 h

In Fig. 8(a), a main absorption band at ca. 340 nm is detected, which corresponds to the $\pi \rightarrow \pi^*$ transition of the aromatic system. This absorption band of product from the test piece surface shifts to a higher value at ca. 360 nm, which provides solid evidence for the formation of a complex between PHEN-OH and Fe²⁺ in acidic media [44]. The spectra of PHEN-NH₂ before and after the test piece immersion exhibit similar behaviors (Fig. 8(b)).

3.8. DFT calculations

The optimized structures and frontier molecular orbital density distributions of PHEN-OH and PHEN-NH₂ are shown in Fig. 9. The corresponding quantum chemical indices of PHEN-OH and PHEN-NH₂ are outlined in Table 6.

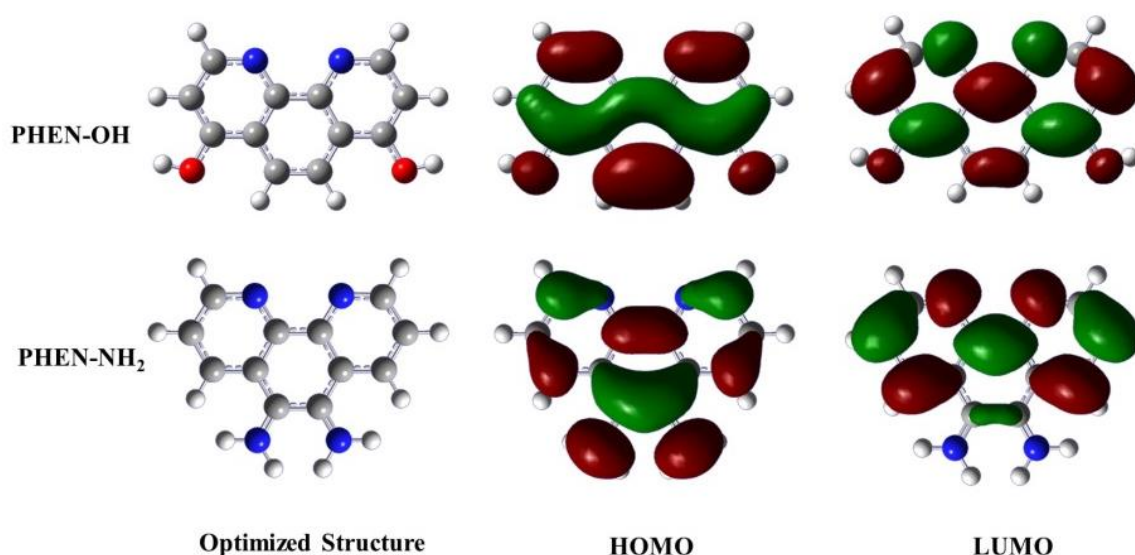


Figure 9. Optimized molecular structures and the frontier molecular orbital density distributions of the investigated PHEN-OH (upper) and PHEN-NH₂ (below).

Table 6. Quantum chemical parameters of PHEN-OH and PHEN-NH₂ inhibitors.

Inhibitor	E_{HOMO} (eV)	E_{LUMO} (eV)	ΔE (eV)	η (eV)	σ (eV ⁻¹)	χ (eV)	ΔN	μ (Debye)
PHEN-OH	-4.18	-1.44	2.74	1.37	0.73	2.81	1.04	10.55
PHEN-NH ₂	-5.89	-1.43	4.47	2.23	0.45	3.66	0.78	3.77

The HOMOs of PHEN-OH and PHEN-NH₂ distribute over the entire molecular, while the LUMOs are well localized at 1,10-Phenanthroline rings in both PHEN-OH and PHEN-NH₂. However, the amino groups in PHEN-NH₂ do not contribute to the LUMOs, which suggests that two amino groups cannot participate in the backward donation of charges during the donor-acceptor interactions between PHEN-NH₂ and Fe [45].

It has been proven that E_{HOMO} is closely related to the electron-donating ability, and the large E_{HOMO} can easily donate an electron to the low-altitude molecular orbital. In contrast, E_{LUMO} is associated with the ability of accepting electrons, and the small E_{LUMO} of the inhibitor indicates the strong ability to accept electrons from the test piece surface. ΔE (energy gap) is also related to the

corrosion inhibition effect, which the low ΔE value involves the strong chemisorption at the interface of the inhibitor molecule and metal [10, 46]. As shown in Table 6, the values of E_{HOMO} based on two phenanthroline derivatives present an increase in the order of PHEN-OH > PHEN-NH₂, while E_{LUMO} and ΔE show a decrease in the order of PHEN-OH < PHEN-NH₂, which indicates that PHEN-OH could more effectively adsorb on the test piece surface to form a complex, which is consistent with the aforementioned viewpoint. In addition, the dipole moment (μ) is one of the key indicators to measure the adsorption capacity. Generally, large μ signifies that the inhibitor can tightly adsorb on the test piece surface. The μ values of PHEN-OH and PHEN-NH₂ are 10.55 D and 3.77 D, respectively, which are larger than that of H₂O (1.85 D), so PHEN-OH and PHEN-NH₂ more easily adsorb than H₂O on the test piece surface to isolate the acidic solution. In short, the calculated results are consistent with experimental data.

4. CONCLUSIONS

The corrosion inhibition performances of PHEN-OH and PHEN-NH₂ for mild steel in acidic media based on electrochemistry and weight loss were investigated, and the results are as follows.

1) Both PHEN-OH and PHEN-NH₂ exhibit highly efficient corrosive performances for mild steel at all investigated concentrations and temperatures. In particular, PHEN-OH exhibits outstanding corrosion inhibition performance for mild steel in 1 M HCl solution, and the inhibition efficiency of PHEN-OH is hardly sensitive to the inhibitor concentration and corrosion system temperature. The maximum inhibition efficiency of PHEN-OH is 97.4%.

2) The thermodynamic parameters suggest that PHEN-OH and PHEN-NH₂ can spontaneously adsorb on mild steel via two adsorption modes with mainly chemisorption, and the process is well fitted with the Langmuir adsorption isotherm.

3) The electrochemical results indicate that both PHEN-OH and PHEN-NH₂ are adsorption-type corrosion inhibitors, which adsorb on metal surfaces. The high electrochemical impedance effectively retards the cathodic process of corrosion.

4) SEM and EDX show that a protective film between PHEN-OH/PHEN-NH₂ and Fe on the surface of mild steel can be formed to inhibit the corrosion in hydrochloric acid solution.

5) The UV-vis spectroscopy reveals that the coordination complexes between the active sites of the novel inhibitor PHEN-OH/PHEN-NH₂ and Fe are formed to impede the metal corrosion.

6) The results of the theoretical calculation are basically consistent with the experimental data.

ACKNOWLEDGMENTS

The authors gratefully acknowledge the National Natural Science Foundation of China (NO: 51634004) and the funding from the Science and Technology Planning Project of Department of Education of Liaoning Province (NO: 2016TSPY09).

References

1. K. Xhanari, M. Finsgar, *RSC Adv.*, 6 (2016) 62833.

2. L. Guo, I. B. Obot, X. Zheng, X. Shen, Y. Qiang, S. Kaya and C. Kaya, *Appl. Surf. Sci.*, 406 (2017) 301.
3. I. B. Obot, A. Meroufel, I.B. Onyeachu, A. Alenazi and A.A. Sorour, *J. Mol. Liq.*, 296 (2019) 111760.
4. M. Chafiq, A. Chaouiki, M. Damej, H. Lgaz and I. M. Chung, *J. Mol. Liq.*, 309 (2020) 113070.
5. X. Li, S. Deng, *Chinese J. Chem. Eng.*, 26 (2018) 2641.
6. Y. Meng, W. Ning, B. Xu, W. Yang, K. Zhang, Y. Chen, L. Li, X. Liu, J. Zheng and Y. Zhang, *RSC Adv.*, 7 (2017) 43014.
7. Y. Ji, B. Xu, W. Gong, X. Zhang, X. Jin, W. Ning, Y. Meng, Wen. Yang and Y. Chen, *J. Taiwan Inst. Chem. Eng.*, 66 (2016) 301.
8. H. Heydari, M. Talebian, Z. Salarvand, K. Raeissi and M. Bagheric, *J. Mol. Liq.*, 254 (2018) 177.
9. A. Dutta, S. Kr. Saha, U. Adhikari, P. Banerjee and D. Sukul, *Corros. Sci.*, 123 (2017) 256.
10. Z. Salarvand, M. Amirnasr, M. Talebian, K. Raeissi and S. Meghdadi, *Corros. Sci.*, 114 (2017) 133.
11. C. M. Fernandes, L. X. Alvarez, N. Escarpini dos Santos, A. C.Maldonado Barrios and E. Ariel Ponzio, *Corros. Sci.*, 149 (2019) 185.
12. Y. Qiang, S. Zhang, B. Tan and S. Chen, *Corros. Sci.*, 133 (2018) 6.
13. L. L. Liao, S. Mo, H. Q. Luo and N. B. Li, *J. Colloid Interf. Sci.*, 499 (2017) 110.
14. S.A. Haladu, S.A. Umoren, S.A. Ali, M.M. Solomon and A.I. Mohammed, *Chinese J Chem. Eng.*, 27 (2019) 965.
15. S. Kumar, H. Vashisht, L. O. Olasunkanmi, I. Bahadur, H. Verma, G. Singh, I. B. Obot and E. E. Ebenso. *Sci. Rep.*, 6 (2016) 30937.
16. P. Alreja, N. Kaur, *RSC Adv.*, 47 (2016) 23169.
17. A. Lotfi, J. L.Manzoori and A. Mohagheghi, *J. Lumin.*, 185 (2017) 132.
18. G. Zhao, J. Zhao, Y. Hu, D. Zhang and X. Li, *Synth. Met.*, 212 (2016) 131.
19. X. Li, G. Zhao, Y. Hu, J. Zhao, Y. Dong, L. Zhou, Y. Lv, H. Chi and Z. Su, *J. Mater. Chem. C.*, 5 (2017) 7629.
20. Z. Zhang, H. Wang, M. Yan, H. Wang and C. Zhang, *Mol. Med. Rep.*, 15 (2016) 3.
21. S. N. Banerjee, S. Misra, *Corrosion*, 45 (1989) 780.
22. N. M. Guan, X. Li and F. Li, *Mater. Chem. Phys.*, 86 (2004) 59.
23. X. Li, L. Tang, L. Li, G. Mu and G. Liu, *Corros. Sci.*, 48 (2006) 308.
24. X. Li, S. Deng and X. Xie, *J. Taiwan Inst. Chem. Eng.*, 45 (2014) 1865.
25. I. B. Obot, N.O. Obiegbedi and A.O. Eseola, *Res. Chem. Intermediat.*, 50 (2013) 2098.
26. N.O. Obi-Egbedi, I.B. Obot, M.I. El-Khaiary, S A Umoren and E E Ebenso, *Int. J. Electrochem. Sci.*, 6 (2011) 5649.
27. N. O. Obi-Egbedi, I. B. Obot and A. O. Eseola, *Arab .J.Chem.*, 7 (2014) 197.
28. X. Lei, H. Wang, Y. Feng, J. Zhang, X. Sun, S. Lai, Z. Wang and S. Kang, *RSC Adv.*, 5 (2015) 99084.
29. X. Li, S. Wu, D. Zhang, Z. Su, P. Lei, Z. Zhang, Z. Hu and W. L, *Synth. Met.*, 160 (2010) 390.
30. X. Luo, C. Ci, J. Li, K. Lin and Y. Liu, *Corros. Sci.*, 151 (2019) 132.
31. N. K. Gupta, P. G. Joshi, V. Srivastava and M. A. Quraishi, *Int. J. Biol. Macromol.*, 106 (2018) 704.
32. M. ElBelghiti, Y. Karzazi, A. Dafali, B. Hammouti, F. Bentiss, I.B. Obot, I. Bahadur and E.E. Ebenso, *J. Mol. Liq.*, 218 (2016) 281.
33. C.M. Fernandes, L. X. Alvarez, N.E. dos Santos, A.C. Maldonado Barrios and E.A. Ponzio, *Corros. Sci.*, 149 (2019) 185.
34. A.Khadiri, R.Saddik, K.Bekkouche, A.Aouniti, B.Hammouti, N.Benchat, M.Bouachrine and R.Solmaz, *J. Taiwan Inst. Chem. Eng.*, 58 (2016) 552.
35. K. Zakaria, N. A. Negm, E. A. Khamis and E. A. Badr, *J. Taiwan Inst. Chem. Eng.*, 61 (2016) 316.
36. E.A. Noor, A.H. Al-Moubaraki, *Mater. Chem. Phys.*, 110 (2008) 145..

37. X. Li, S. Deng, T. Lin, X. Xie and G. Du, *Corros. Sci.*, 118 (2017) 202.
38. O.L. Riggs, *Corrosion.*, 31 (1975) 413.
39. H. M. Abd El-Lateef, *Corros. Sci.*, 92 (2015) 104.
40. J. Aljourani , K. Raeissi and M.A. Goloza, *Corros. Sci.*, 51 (2009) 1836.
41. S.S.D.A.A. Pereira, M.M Pêgas, T.L. Fernández, M.Magalhães, T.G Schöntag, D. C Lago, L.F.D. Senna and E. D'Elia, *Corros. Sci.*, 65 (2012) 360.
42. V.V. Torres, V.A. Rayol, M. Magalhaes, G.M. Viana, L.C.S. Aguiar, S.P. Machado, H. Orofino and E. D'Elia, *Corros. Sci.*, 79 (2014) 108.
43. X. Wang, H. Yang and F. Wang, *Corros. Sci.*, 53 (2011) 113.
44. M. Abdallah, M. M. El-Naggar, *Corros. Sci.*, 139 (2018) 430.
45. C. Verma, L. O. Olasunkanmi, I. B. Obot, E. E. Ebenso and M. A. Quraishi, *RSC Adv.*, 6 (2016) 53933.
46. M. Bouklah, N. Benchat, B. Hammouti, A. Aouniti and S. Kertit, *Mater. Lett.*, 60 (2006) 1901.